Microstructure of epitaxial MnAs films on GaAs(001): An *in situ* x-ray study

B. Jenichen,[a] D. Satapathy, W. Braun, L. Däweritz, and K. H. Ploog
Paul-Drude-Institut für Festkörperelektronik, Hausvogteiplatz 5–7, D-10117 Berlin, Germany

(Received 2 June 2004; accepted 16 August 2004)

We present an analysis of thin MnAs films on GaAs(001) by the x-ray grazing incidence diffraction during molecular-beam epitaxy and immediately after deposition near the growth temperature. Separate MnAs peaks are detected for average thicknesses starting from ≈1 monolayer, indicating the formation of a relaxed MnAs lattice. The variation of the position and shape of the MnAs peaks during growth yields the time dependence of relaxation and island sizes. The MnAs domains of different orientations are detected and their amount is analyzed quantitatively. A line broadening due to the size and strain effects is observed. Both the effects are separated for each of the main directions along the interface. The lateral domain sizes of 10–40 nm and strain values of 0.2%–0.6% are found in the MnAs films. We find that the positions of the misfit dislocations at the interface are correlated. © *2004 American Institute of Physics*. [DOI: 10.1063/1.1804621]

I. INTRODUCTION

The combination of magnetic and semiconducting materials leads to the development of semiconductor devices utilizing the spin of the carriers.[1–4] At room temperature, MnAs on GaAs is a combination of a ferromagnet and a semiconductor.[5] The interface between MnAs and GaAs is found to be smooth and of rather good structural perfection. On the other hand, the misfit between the MnAs and the GaAs lattices is near 7.5% along the *a* axis and about 30% along the *c* axis of MnAs. Thus, MnAs on GaAs is an example of an extreme heteroepitaxy, which results in the films containing relatively high defect densities like the misfit dislocations at the heterointerface and threading dislocations in the bulk of the film.[6,7]

The x-ray diffraction peaks of such films are broadened due to the lattice defects. The methods developed for the analysis of line broadening[8–18] are valuable tools for the microstructural characterization of these epitaxial layers. Monochromatized synchrotron radiation is well suited for the line-broadening analysis, because the apparatus function is narrow.[16] The method of grazing incidence diffraction[19,20] allows a direct access to lateral parameters, whereas the conventional diffraction, especially in the symmetrical geometry, is more sensitive in the direction perpendicular to the interface.

MnAs layers undergo two structural phase transitions when being cooled down from the growth temperature 250 °C to room temperature. At 125 °C, a structural second-order phase transition occurs from the hexagonal to the orthorhombic phase. At approximately 40 °C, a first-order paramagnetic–ferromagnetic phase transition takes place accompanied by a discontinuity of the lattice parameter *a* in the hexagonal plane.[21,22] Due to these phase transitions, the strain state of the film during deposition cannot be determined in the *ex situ* experiments. *In situ* reflection high-energy election diffraction (RHEED) and reflectance difference spectroscopy in combination with scanning tunneling microscopy (STM) measurements during MnAs growth by molecular-beam epitaxy (MBE) on GaAs(001) with a 2° miscut have been published in Ref. 23. Here, we report the *in situ* grazing incidence x-ray diffraction (GID) measurements *during* the first stages of thin film growth on exactly oriented GaAs(001) and further characterization of the film after the growth at a temperature of 200 °C, i.e., well above the phase transitions.

II. EXPERIMENT

The *in situ* x-ray measurements were performed at the wiggler beamline U125/2 KMC at the storage ring BESSY (Berlin, Germany) using a double-crystal Si(111) monochromator. The energy of the radiation was 12 keV. A six-circle x-ray diffractometer coupled with MBE system[24] was used for the grazing incidence diffraction measurements. The acceptance angle of the detector was 0.1°, both parallel and perpendicular to the surface. The ω (and $\omega/2\Theta$) scans were performed in the grazing incidence geometry by a rotation of the sample (together with the detector) around the surface normal of the sample, keeping the incident and the exit beams under small glancing angles with respect to the sample surface.[19]

An average MnAs effective layer thickness was determined after the growth and the *in situ* measurements by the subsequent *ex situ* x-ray reflectivity using a Panalytical X-Pert system with a Ge(220) hybrid monochromator and the corresponding software.

The MnAs layers were grown by the solid source MBE in the system mentioned earlier. Commercially available GaAs(001) epi-ready substrates without an intentional miscut were used. The temperature was measured by a thermocouple near the plate of the sample holder. A thick GaAs buffer layer was grown first at 550 °C under the RHEED control.[25,26] Then, the MnAs layer was grown on the c(4 × 4)-reconstructed GaAs template at 250 °C with a very low growth rate of 0.5 nm h^{-1}, under As-rich conditions. The MBE growth was stopped just before a continous film with a smooth surface had developed in order to compare the MnAs

[a]Electronic mail: jen@pdi-berlin.de

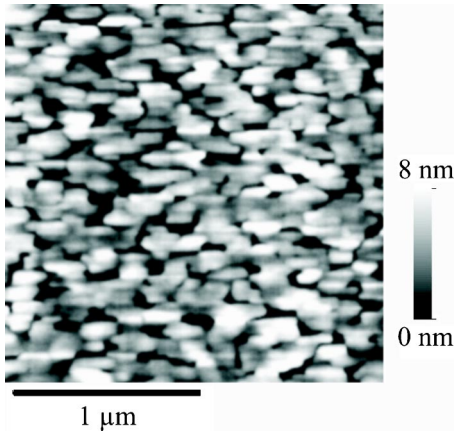

FIG. 1. Atomic force micrograph of the sample surface after the growth was finished, revealing an MnAs island pattern on the GaAs surface.

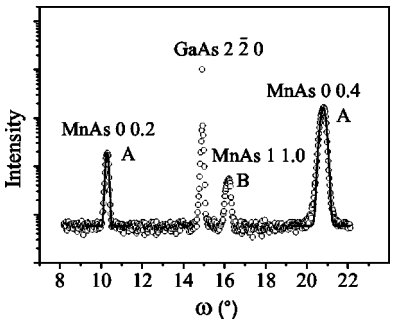

FIG. 3. X-ray grazing incidence diffraction curve ($\omega/2\Theta$ scan, circles) measured at a substrate temperature of 200 °C along the GaAs $[1\bar{1}0]$ direction with the GaAs $2\bar{2}0$ substrate and the MnAs 00.2 and 00.4 layer reflections (from the domains in *A* orientation). The MnAs 11.0 reflection from the domains in *B* orientation is also visible. The MnAs 00.2 and 00.4 peaks are fitted to the Gaussian functions (solid lines).

island sizes measured by the atomic force microscopy (AFM) with the results of the of x-ray measurements. The growth rate was kept constant during the experiment. A comparison of the growth times with the final time and the final layer thickness were used for the determination of the thickness of the growing layer at any time during the growth.

The x-ray GID measurements after the growth were performed at a temperature of 200 °C, in order to prevent the evaporation of As from the walls of the MBE chamber, because the sample environment was not cooled anymore at that time.

III. RESULTS AND DISCUSSION

The main result of our experiments is the *in situ* observation of the grazing incidence x-ray diffraction peaks *during* the MBE growth, which change their widths and their positions in dependence of the growth time (see Fig. 5). But for a more detailed understanding, we first present some preliminary information about the growth morphology of the MnAs film and the epitaxial relationship between the MnAs and the GaAs(001) substrates.

Figure 1 displays an overview of the surface of our sample seen by the AFM after the growth. We find an island pattern with a size anisotropy. The feature sizes are in the range of about 100–300 nm. The AFM micrograph clearly reveals, an island formation, but it does not show evidence if the coalescence of the islands has already occurred. Later, we will compare the island sizes obtained by the *ex situ* AFM and by the *in situ* grazing incidence diffraction. The height of the features in the AFM micrograph is 8 nm. From the final film thickness of 20 ± 0.5 nm obtained by the *ex situ* x-ray reflectivity measurements, we conclude that the trenches do not reach the substrate surface in this AFM micrograph and so the film is probably already closed.

Figure 2 shows a schematic view of the epitaxial relationship of the MnAs layer and the GaAs(001) substrate. At 250 °C, MnAs has the hexagonal NiAs structure, because this temperature is clearly above the second-order phase transition found at 125 °C. The MnAs film orientation with the *c* axis [00.1] parallel to GaAs $[1\bar{1}0]$ is called the *A* orientation and the *c* axis of the film parallel to GaAs [110] is referred to as the *B* orientation.[27] We find a rather limited amount of *B* domains in the MnAs film and can demonstrate the sensitivity of the grazing incidence diffraction method which, in principle, would allow to analyze the competition between the two orientations during growth.

Figures 3–5 demonstrate the *in situ* measurements ($\omega/2\Theta$ scans) of the in-plane MnAs diffraction peaks together with the corresponding substrate reflections performed during and immediately after the growth at substrate temperatures of 250 and 200 °C, respectively. Figures 3 and

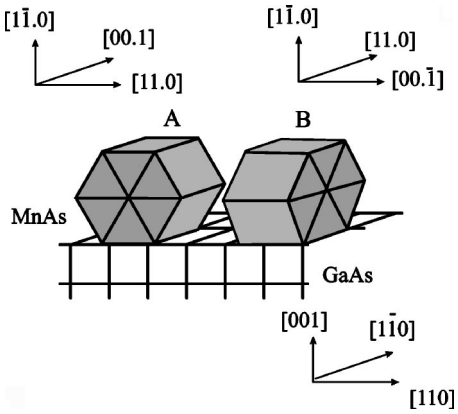

FIG. 2. Schematic view of the epitaxial relationship of MnAs on GaAs(001). The *A* and *B* orientations of the MnAs film are shown.

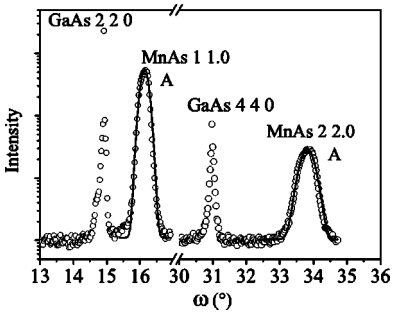

FIG. 4. X-ray grazing incidence diffraction curves ($\omega/2\Theta$ scans, circles) measured at a substrate temperature of 200 °C along GaAs [110] with the GaAs 220 and 440 substrates and the MnAs 11.0 and 22.0 layer reflections of the domains in *A* orientation. The MnAs 11.0 and 22.0 peaks are fitted to the Gaussian functions (solid lines).

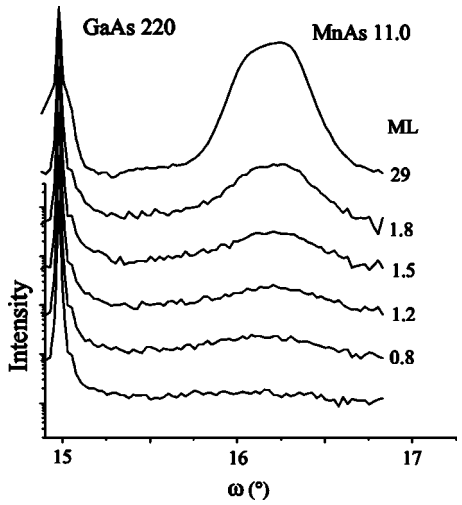

FIG. 5. X-ray grazing incidence diffraction curves ($\omega/2\Theta$ scans) measured at a substrate temperature of 250 °C along GaAs [110] with the GaAs 220 substrate and the MnAs 11.0 layer reflections during the growth of the MnAs film. The approximate layer thicknesses (island heights) determined from a comparison of the corresponding growth times with the overall growth time and the final layer thickness are indicated. A distinct MnAs 11.0 peak is observed already at an average thickness of ≈1 monolayer (ML). Both the position and the half width of the MnAs 11.0 peak change with the layer thickness.

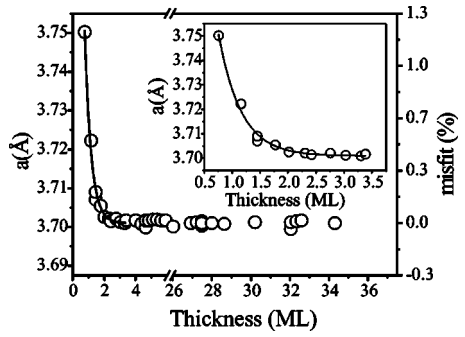

FIG. 6. Lattice parameter a as a function of the thickness of the growing layer. The line fitted to the data is an exponential decay function. The inset presents an enlarged plot of the initial phase of the growth. The MnAs films is already fully relaxed at a thickness of 2.5 monolayers (ML). The corresponding error bars are smaller than the symbols.

4 show all the different reflections we observed in the GID geometry, whereas Fig. 5 demonstrates the *in situ* measurements *during* the MBE growth experiment. The scan represented in Fig. 3 is directed along GaAs $[1\bar{1}0]$. The GaAs $2\bar{2}0$ substrate and the MnAs 00.2 and 00.4 layer reflections from the *A*-oriented domains are most pronounced. Figure 4 shows the diffraction measurements along GaAs [110] with the GaAs 220, 440 substrate, and the MnAs 11.0, 22.0 layer reflections of the MnAs *A* domains. The detection of several diffraction orders allows for a more detailed analysis of the diffraction curves. We observe a considerable broadening of the MnAs 00.4 peak compared to the MnAs 00.2 reflection (Fig. 3), as well as the broadening of the MnAs 22.0 peak in comparison to the MnAs 11.0 peak (Fig. 4). Gaussian fits (solid lines) were applied to the MnAs peaks. Slight asymmetries are neglected in this work. Despite the small film thickness of 20 ± 0.5 nm, the measurements of the lattice spacings near the growth temperature can be performed using the GaAs lattice as a reference. Combining the data from the MnAs 11.0, 22.0, 00.2, and 00.4 reflections, we obtain the MnAs film lattice parameters parallel to the interface at 200 °C as $a=3.70$ Å and $c=5.79$ Å. These values match those measured in the bulk MnAs at the same temperature, $a=3.70$ Å and $c=5.77$ Å,[21] i.e., the layer at the final thickness of 20 nm is almost completely relaxed near the growth temperature.

The MnAs 11.0 reflection from the MnAs domains in *B* orientation is also visible in Fig. 3. From the comparison of the integrated intensities of the 11.0 reflections of the *A* and *B* domains in Figs. 4 and 3, respectively, we establish a content of 93.1% of the *A* domains in the layer. In the remaining part of the paper, we consider the *A* domains in more detail.

The main advantage of our experimental setup is the possibility to perform the *in situ* x-ray measurements. Figure 5 shows the $\omega/2\Theta$ scans taken *during* the MBE film growth. A distinct MnAs 11.0 peak is observed already at an average thickness of ≈1 monolayer (ML), indicating the formation of the relaxed MnAs islands, which are not coherent on the GaAs substrate lattice anymore. The position and the half width of the MnAs 11.0 peak change. From the peak positions and widths of these scans, the *in situ* values of the average island (domain) sizes and the *a* parameter parallel to the interface can be calculated. The approximate layer thicknesses (island heights) determined by a comparison of the corresponding growth times with the overall growth time and the final thickness are also given in Fig. 5. The thicknesses given in Figs. 6 and 8 are also based on this comparison. Figure 6 contains a plot of the in-plane lattice spacing a, parallel to the interface, versus the thickness of the growing layer. During the growth, we observe a further relaxation of this lattice parameter by 1%. The MnAs film is already fully relaxed at a thickness of 2.5 ML.

Now, we consider the determination of the average island (domain) sizes together with the strain in these domains. During the first time of the growth, the thin-growing film probably consists of many separate islands,[23] which coalesce during a later stage of the film growth. At the boundaries between the originally separate islands, we can expect a higher defect density. These facts support a model of coherently diffracting domains divided by defected regions.

The angular spread of the grazing incidence x-ray ω scans of our films is near 1°. The corresponding breadths $\Delta\omega$ are given in Table I for the 11.0 and the 00.2 reflections. The integral breadths of all the MnAs peaks in the $\omega/2\Theta$ scans are smaller than those of the ω scans, but all larger than that of the apparatus function, which we approximate by a Gaussian of 0.1° integral breadth.[16] In our range of the Bragg angles, the breadth of the apparatus function can be considered to be constant.[18] The peak shapes of the $\omega/2\Theta$ scans are Gaussian, so that we can subtract the breadth of the apparatus function β_g from that of the measured curve β_h by

$$(\beta_f)^2 = (\beta_h)^2 - (\beta_g)^2, \tag{1}$$

in order to obtain the breadth β_f of the physically broadened profile.[12,15,28] We assume that the layer consists of coherently diffracting domains separated by areas with a higher defect density.[12,23] These domains are twisted around the surface

TABLE I. Some microstructural properties of the 20-nm-thick MnAs layer on GaAs(001). The $\Delta\omega$ are the mosaic spreads of the twist angle of the domains obtained directly from the widths of the ω scans across the 00.2 and the 11.0 diffraction maxima. The average domain sizes l and strains e along two perpendicular directions in the interface between MnAs and GaAs are calculated from the integral breadths of the physically broadened profiles of the $\omega/2\Theta$ scans. The corresponding correlation parameters γ of the positions of the dislocations are estimated from a comparison with the theory for the randomly positioned dislocations.

Direction along IF	$\Delta\omega$ (°)	l (nm)	e (%)	γ
00.1	0.7	35	0.60	0.11
11.0	0.8	12	0.22	0.03

normal by different angles yielding a broad rocking curve in the grazing incidence diffraction.[29–31] The ω scans show the orientational distribution of the different diffracting domains. On the other hand, $\omega/2\Theta$ scans are broadened due to the finite size of the diffracting domains and due to the inhomogeneous deformations inside the domains. In order to separate the size and strain broadening effects, we assume that the integral breadth of the physically broadened profile β_f of our sample consists of the size and strain components β_S and β_D. The size component β_S does not depend on the diffraction angle. The strain component β_D increases linearly with the order of reflection.[12,15] We apply the reciprocal lattice notation: $|d^*|=1/d=2\sin(\Theta)/\lambda$ is the absolute value of the reciprocal-lattice vector and $\beta_f^*=\beta_f\cos(\Theta)/\lambda$. Θ is the diffraction angle and λ is the wavelength. The integral breadth of the physically broadened line profile is $\beta_f(2\Theta)=A/I_0$, where A is the integral intensity and I_0 is the peak intensity of the corresponding maximum.

For a Gaussian peakshape, we have to sum the squares of the two contributions[12,18]

$$(\beta_f^*)^2=(\beta_S^*)^2+(\beta_D^*)^2=(\beta_S^*)^2+(2e\cdot d^*)^2, \tag{2}$$

where

$$e=\beta_D^*/2d^*=\Delta d/d \tag{3}$$

is the strain,[9,17,18] which can be interpreted as a variation of the d spacing within the domains. A Gaussian stress distribution was assumed. According to (2), the plot of $(\beta_f^*)^2$ over $(d^*)^2$ should give a straight line[13,18] Such a plot, as shown in Fig. 7, is a Williamson-Hall (WH) plot in a reciprocal-lattice representation. We could measure only two orders of reflections in the grazing incidence diffraction geometry. The intersection with the ordinate axis leads to β_S^*. It yields the size

$$l=1/\beta_S^*. \tag{4}$$

(see Table I). This is the volume-weighted size of an average domain (or island) in the direction of the diffraction vector, which is in our case, parallel to the interface. The strain e is obtained from the slope of the WH plot. The results are summarized in Table I.

Figure 8 shows the in-plane domain (island) size l in dependence of the thickness of the growing layer. For thin layers, we expect the MnAs islands on the GaAs surface and for thicker layers, the x rays probe a domain size. The domain sizes were calculated using Eq. (4), assuming that the strain e (3) remains constant during the growth. This assumption holds for the film thicknesses above 2.5 monolayer (ML, full relaxation, see Fig. 6), but even for lower thicknesses, the error is increased only by ≈2%. The average island sizes measured here by the *in situ* x-ray diffraction during the MnAs growth on exactly oriented GaAs(001) are of the same order of magnitude as the island sizes obtained by the STM in Ref. 23, for the growth on GaAs(001) with a 2° miscut (after the growth interruption and transferring of the quenched sample to the STM chamber).

For a more detailed analysis of the integral breadths of the MnAs peaks, we used the program BREADTH,[17] which calculates the domain sizes and the strain. Figure 9 shows, as a result of this program, the volume-weighted distribution function (circles) of the size l along MnAs [00.1]. The line is a fit by a lognormal function. The width of this function gives information about the range of sizes, which we can expect for an average size of 35 nm±10 nm. In principle the shape of the distribution function can be related to the

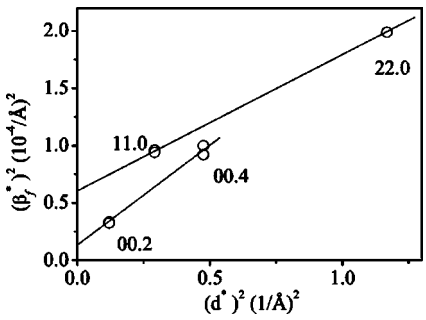

FIG. 7. Williamson-Hall plot in the reciprocal-lattice representation for the Gaussian line profiles. d^* is the reciprocal-lattice vector and $\beta_f^*=\beta_f\cos(\Theta)/\lambda$, where β_f is the integral breadth of the physically broadened profile.

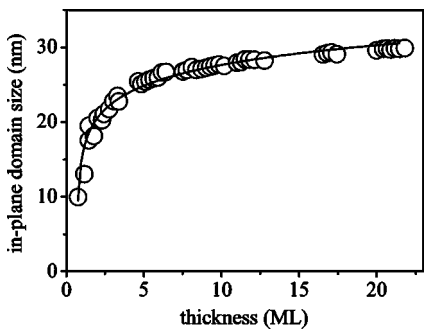

FIG. 8. Average in-plane domain size l vs the layer thickness measured in the monolayers (ML) during the growth. The size was calculated according to Eq. (4).

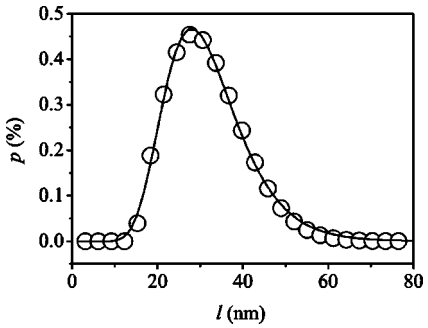

FIG. 9. Volume-weighted distribution function (circles) along MnAs [00.1]. The line is a fit by a lognormal function. This function demonstrates the possible fluctuations of the domain sizes.

growth mode of the film.[32] As expected for the Gaussian line profiles, the hook effect occurs in the Warren-Averbach method, i.e., for small sizes, the probability p falls below zero.[12,17] This has no physical meaning, and so the probability p is set to zero in this range. For our sample, this could point to a minimal domain size l along MnAs [00.1] of about 10 nm.

The feature sizes on the AFM micrograph, shown in Fig. 1, are in the range of about 100–300 nm, i.e., they are larger by a factor of 10, compared with the domain size given in Table I. This indicates that the coalescence of islands has already taken place during the final stage of the growth. The x-ray measurement is probably probing the size of the originally separate islands.

Apart from the size of the coherently scattering domains, we can discuss also the origin of the strain. This can be done by considering in more detail the influence of the misfit dislocations and their periodical arrangement in the two perpendicular directions along the interface. We assume for the analysis of the scans along GaAs[110] and MnAs[11.0], shown in Fig. 4, that the strain is mainly due to the misfit dislocations with the dislocation lines parallel to the c axis of the MnAs lattice. These dislocations are quasiperiodically arranged edge dislocations.[6,26] The absolute value of their Burgers vector is $|b|=a=0.37$ nm. We have measured an in-plane lattice-parameter change due to the misfit relaxation $\Delta a/a=-0.075$, i.e., the MnAs layer is almost completely relaxed on the GaAs substrate. The linear density of the misfit dislocations due to this relaxation can be calculated by[33]

$$\rho = (|\Delta a/a|)/b. \tag{5}$$

We obtain $\rho=0.2/\text{nm}$, i.e., the average distance between the dislocations is near 5 nm. For the randomly positioned dislocations at the interface, the halfwidth of the diffraction curve in the reciprocal-lattice notation can be estimated as $\beta^*_{\text{rand}} \approx Qb\sqrt{\rho/t} = Q\sqrt{|\Delta a/a|(b/t)}$.[34] Here, $Q=2\pi d^*$ is the scattering vector and $t\cong 20$ nm is the thickness of the epitaxial layer. For the [11.0] reflection, we get $\beta^*_{\text{rand}}=0.123$ Å^{-1}. The widths observed in the experiment are considerably lower. We measured $\beta^*_D=0.0041$ Å^{-1} (obtained from Fig. 7 for the same reflection). Taking into account the correlations in the positions of the dislocations leads us to narrower peak widths.[34] The ratio $\beta^*_D/\beta^*_{\text{rand}}$ yields the correlation parameter $\gamma\approx 0.03$, which describes the fluctuations of the number of dislocations: $\gamma=\langle(\Delta\rho)^2\rangle/\rho$, here, $\Delta\rho$ is the variation of the mean number of dislocations in some interval.[34] This small value of γ indicates that the defects are well correlated in the position (see also Table I). Superstructure satellites due to the periodic arrangement of the dislocations were observed along the 11.0 direction.[26]

In the perpendicular direction, i.e., along the MnAs c axis, a coincidence lattice is observed:[6,7] every fourth {00.2} MnAs plane fits every sixth {220} GaAs plane forming a commensurate interface region. This 4/6 ratio reduces the lattice mismatch from 30% to about 5%. The deviation from the exact coincidence is accomodated by the defects characterized by two additional MnAs{00.2} planes connected to two additional GaAs{220} planes in one coincidence lattice mesh [see Fig. 2(c) in Ref. 6], the so-called extended secondary dislocations. The remaining misfit is released, if such an extended dislocation is placed in every third unit of the coincidence lattice, i.e., every 3.42 nm. These extended dislocations lead to an inhomogeneous deformation field near the interface, similar to the real dislocations observed in the perpendicular direction, causing the broadening of the x-ray diffraction peaks. We define formally an effective Burgers vector b of such an extended dislocation. The absolute value of its component along the interface is $|b_{\text{IF}}|=c_{MnAs}-a_{GaAs}/\sqrt{2}=0.171$ nm. Then, we get for the [00.4] reflection a value of $\beta^*_{\text{rand}}=0.09$ Å^{-1}. Our own measurements give a value of $\beta^*_D=0.01$ Å^{-1} for the same reflection. The ratio $\beta^*_D/\beta^*_{\text{rand}}$ yields a correlation parameter $\gamma\approx 0.11$ for the extended dislocations, which are superimposed onto the coincidence lattice. This value is larger than for the 11.0 direction, i.e., the defects are less correlated, the relative position fluctuations are larger. No superstructure satellites were observed along the 00.1 direction.[26]

IV. SUMMARY

In conclusion, we have performed an *in situ* microstructural analysis during and after the MBE growth of a MnAs film on GaAs using the grazing incidence diffraction of x-rays. A separate MnAs peak was detected for an average thickness of ≈1 ML and above, indicating the formation of a relaxed MnAs lattice. We determined the final content of *A*- and *B*-oriented domains, evaluated directly the angular spread of the twist angle of the *A* domains, and measured both the lateral lattice parameters of the MnAs film near the growth temperature. A fully relaxed layer was found at the final thickness of about 20 nm. We determined the island (domain) sizes and the lateral lattice parameter *in situ* during the epitaxial growth, measured the strain inside the domains, and found estimates for the correlation parameters γ of the dislocation arrays. We established a full relaxation already for an average thickness of the growing MnAs film as small as 2.5 ML. The coalescence of the originally separate islands was observed at the final stage of the epitaxial growth.

ACKNOWLEDGMENTS

The authors thank V. M. Kaganer and A. Trampert for the critical reading of the manuscript and the helpful discussions, and X. Guo for his support during the experiments.

Part of this work was sponsored by the Bundesministerium für Bildung und Forschung of the Federal Republic of Germany.

[1]G. A. Prinz, Science **54**, 17638 (1996).
[2]M. Tanaka, J. Cryst. Growth **201–202**, 660 (1999).
[3]H. Ohno, Physica E (Amsterdam) **6**, 702 (2000).
[4]M. Ramsteiner, H. Zhu, A. Kawaharazuka, H.-Y. Hao, and K. H. Ploog, Adv. Solid State Phys. **42**, 95 (2002).
[5]M. Tanaka, J. Harbison, M. C. Park, Y. S. Park, T. Shin, and G. M. Rothberg, J. Appl. Phys. **76**, 6278 (1994).
[6]A. Trampert, F. Schippan, L. Däweritz, and K. H. Ploog, Appl. Phys. Lett. **76**, 2461 (2001).
[7]A. Trampert, Physica E (Amsterdam) **13**, 1119 (2002).
[8]P. Scherrer, Nachr. Ges. Wiss. Goettingen, Math.-Phys. Kl. **2**, 98 (1918).
[9]A. R. Stokes and A. J. C. Wilson, Proc. Phys. Soc. London **56**, 174 (1944).
[10]B. E. Warren and B. L. Averbach, J. Appl. Phys. **21**, 595 (1950).
[11]B. E. Warren and B. L. Averbach, J. Appl. Phys. **23**, 497 (1952).
[12]B. E. Warren, *X-Ray Diffraction* (Addison-Wesley Pub. Co., Reading, Mass., 1969).
[13]G. K. Williamson and W. H. Hall, Acta Metall. **1**, 22 (1953).
[14]W. H. Hall, Proc. Phys. Soc., London, Sect. A **62**, 741 (1949).
[15]H. P. Klug and L. E. Alexander, *X-Ray Diffraction Procedures* (Wiley, New York, 1974).
[16]T. C. Huang, M. Hart, W. Parrish, and N. Masciocchi, J. Appl. Phys. **61**, 2813 (1987).
[17]D. Balzar and H. Ledbetter, Adv. X-Ray Anal. **39**, 457 (1997).
[18]J. I. Langford, *Industrial Applications of X-Ray Diffraction* (Marcel Dekker Inc., New York, 2000), p. 751.
[19]W. C. Marra, P. Eisenberger, and A. J. Cho, J. Appl. Phys. **50**, 6927 (1979).
[20]H. Dosch, B. W. Batterman, and D. C. Wack, Phys. Rev. Lett. **56**, 1144 (1986).
[21]B. T. Willis and H. P. Rooksby, Proc. Phys. Soc. London, Sect. B **67**, 290 (1954).
[22]R. H. Wilson and J. S. Kasper, Acta Crystallogr. **17**, 95 (1964).
[23]M. Kästner, F. Schippan, P. Schützendübe, L. Däweritz, and K. H. Ploog, J. Vac. Sci. Technol. B **18**, 2052 (2000).
[24]B. Jenichen, W. Braun, V. M. Kaganer, A. G. Shtukenberg, L. Däweritz, C. G. Schulz, and K. H. Ploog, Rev. Sci. Instrum. **74**, 1267 (2003).
[25]F. Schippan, A. Trampert, L. Däweritz, and K. H. Ploog, J. Vac. Sci. Technol. B **17**, 1716 (1999).
[26]D. K. Satapathy, B. Jenichen, W. Braun, V. M. Kaganer, L. Däweritz, and K. H. Ploog, J. Vac. Sci. Technol. B **22**, 2079 (2004).
[27]L. Däweritz *et al.*, J. Cryst. Growth **227-228**, 834 (2001).
[28]J. I. Langford, J. Res. Natl. Inst. Stand. Technol. **846**, 110 (1993).
[29]V. Srikant, J. S. Speck, and D. Clarke, J. Appl. Phys. **82**, 4286 (1997).
[30]Y. J. Sun, O. Brandt, T. Y. Liu, A. Trampert, K. H. Ploog, J. Bläsing, and A. Krost, Appl. Phys. Lett. **81**, 4928 (2002).
[31]J. E. Ayers, J. Cryst. Growth **135**, 71 (1994).
[32]D. D. Eberl, V. A. Drits, and J. Srodon, Am. J. Sci. **298**, 499 (1998).
[33]S. N. G. Chu, A. T. Macrander, K. E. Strege, and J. W. D. Johnston, J. Appl. Phys. **57**, 249 (1985).
[34]V. M. Kaganer, R. Köhler, M. Schmidbauer, R. Opitz, and B. Jenichen, Phys. Rev. B **55**, 1793 (1997).